Geometry optimization for multi-inlet vortex photoreactor for CO_2 reduction

J. Valdés[a], J. L. Domínguez-Juárez[b,c], R. Nava[a], Á. Cuán[a], and C. M. Cortés-Romero[d,*]

[a]*Facultad de Ingeniería, Universidad Autónoma de Querétaro, Santiago de Querétaro, México.*
[b]*Centro de Física Aplicada y Tecnología Avanzada, Universidad Nacional Autónoma de México-Querétaro, México.*
[c]*Cátedras CONACyT, Centro de Física Aplicada y Tecnología Avanzada, Universidad Nacional Autónoma de México, Juriquilla, Querétaro 76230, México.*
[d]*Facultad de Química, Universidad Autónoma de Querétaro, Santiago de Querétaro, México,*
[*]*e-mail: carlos.cortes@uaq.mx.*

Received 23 July 2021; accepted 2 September 2021

Process optimization of multiphase chemical and/or photochemical reactor means a challenge not only at laboratory scale but also while scaling-up is intended towards industrial applications. Using computational tools, such as Computational Fluid Dynamics, is essential to assess the transport limitations of the heterogeneous process to verify the kinetic regime while the reaction and the reactor engineering are studied. Computational Fluid Dynamics, together with Genetic Algorithms, have been currently applied to verify fluid behavior and turbulence. The latter device has been self-designed and is planned to be constructed for CO_2 reduction. The results of the Computational Fluid Dynamics simulations are presented and discussed to optimize the operation of a multi-inlet vortex photoreactor. By considering the catalytic particle features, the residence time distribution in the multi-inlet photoreactor has been verified and optimized.

Keywords: Genetic algorithm; residence time; turbulence intensity; computational fluid dynamics.

DOI: https://doi.org/10.31349/RevMexFis.68.020601

1. Introduction

The growing demand for energy sources to sustain the lifestyle of today's societies has brought consequences to the environment, as well as public health problems in industrialized cities [1]. The use of fossil fuels as the main source of energy, leads to the generation of greenhouse gases, where more than 77% of the total concentration of anthropogenic gases corresponds to CO_2 [2]. Despite the efforts and results achieved by the so-called renewable energies, oil and coal continue to be the principal energy sources, more than 60% of the energy produced comes from these two sources [3]. Different approaches have been proposed and evaluated to mitigate the effects of CO_2, from capture and storage, to its reuse and conversion to high-value chemicals [4]. The reuse of CO_2 for fuel production can be achieved through electrochemistry, traditional catalysts, and biological conversions [5–8]. However, these processes require considerable energy consumption, and result in high operating costs [9, 10]. The transformation of solar energy into chemical bonds provides long-term energy storage [11, 12], whereas the photoreduction of CO_2 to hydrocarbons is one of the breakthroughs in the field of photocatalysis. The materials used in the process of photocatalysis are responsible for absorbing sunlight, this absorption can create electron-hole pairs, that can migrate to the surface where they can be used for H_2O dissociation and CO_2 reduction [13–17]. The most common CO_2 transformation leads to a product such as methane, methanol, formaldehyde, acid formic, etc., always demanding a high amount of energy since these are endergonic and non-spontaneous chemical reactions [18]. Although there have been multiple studies regarding the synthesis of efficient and stable photocatalyst [19, 20], only a few studies focus their attention on reaction engineering, as well as obtaining the optimal conditions for the reaction and the photoreactors design [21–26].

Two reactor configurations are used extensively for applications in CO_2 reduction with photocatalytic methods, the continuous flow system and the batch system. The batch system is one of the most reported, however, its photocatalytic efficiency is low, becoming imprecise when compared to other methods [27]. The key limitation of the batch reactor system is the accumulation of products inside the reactor chamber for a defined time, which can lead to changes in the concentration of the reactants and reabsorption at the surface of the photocatalyst. Although continuous-flow reactors have better efficiency, the production of compounds is inadequate due to the short residence time of the reactants inside the reactor chamber, reducing the contact time with the photocatalytic material [28, 29]. In this sense, the optimization of the residence time for continuous flow reactors, becomes a difficult problem to solve, as well the study of the fluid dynamics and the mass transfer, due to the geometric dependence presented by the fluid dynamics inside the reactor.

The optimization problem by deterministic methods for systems whose analytical representation cannot be solved traditionally, numerical methods and stochastic algorithms become a great alternative. One of the most popular stochastic methods, which belongs to the family of evolutionary algorithms, is the Genetic Algorithm (GA) [30]. This concept

was first formalized by Holland [31], and later extended by De Jong for functional optimization [32]. GA uses search strategies inspired by the Darwinian notion of natural selection and evolution. During an optimization by GA, a set of solutions are chosen randomly, this set generates an offspring with the best characteristics of the previous population. This generation of offspring and selection is used recursively to get an optimum solution [33].

On other hand, Computational Fluid Dynamics (CFD) is a well-established tool for numerous areas of science and engineering [34–36]. CFD uses numerical methods and empirical approximations to solve the Navier-Stokes equations, and due to the development of numerical methods and advances in computational technology, there exists a growing confidence in the results of these computational methods. From the reactor design point of view, in the case of gas-solid reactors, the geometric complexity restricts detailed modeling of their fluid dynamics and, therefore, their optimization. In this sense, tools such as CFD, bring a trustworthy tool for solving fluid dynamics in gas-solid reactor systems [37–41].

In the present work, GA are used to maximize the residence time of the reactant phase inside a multi-inlet vortex photoreactor. CDF is used to solve the fluid dynamics inside each individual in the population of GA. The objective function as well as the statistics of residence time is reported and compared to the classic geometric configuration of multi-inlet vortex reactors. An analysis of turbulent intensities inside the photoreactor was implemented to determine the best operational conditions.

2. Methology

2.1. Optimization Process of the Prototype Reactor

2.1.1. Genetic Algorithm

The importance of using the Genetic Algorithm in the present work lies in the wide range of possibilities to build a reactor device. Logically, there is a large number of configurations to arrange and set the reactant inlet, the product outlet as well as the catalyst support within the reactor vessel. This set of parameters must be evaluated which makes the process time and computer demanding. To initialize the reactor configuration selection, are required design values currently established, and afterward the algorithm randomly generates and evaluates the best generation of results, which are fit according to the objective function.

The implemented GA consists of six main steps, four of them correspond to the evolutionary loop, where the selection of parents, crossing, mutations, creation of offspring and the selection of individuals for the next generation takes place; the other two steps correspond to the initialization and termination of the evolutionary loop. The algorithm can find a local minimum of a real and real-valued objective function $f(\vec{x})$. In cases where there is a direct comparison with deterministic methods of optimization, like Lagrange or dual, it is known that GA approximates very well to a global optimum (global maximum or minimum) [42]. However, there is no mathematical proof that assures that GA reaches a global optimum [43, 44]. In this sense, the so-called local minimum (optimum) is described by the currently obtained result applying GA. The following are the six steps implemented in GA:

1. Initialization. In this step, the first population (t_0) is generated with N numbers of individuals, each individual has a specific gene which is a vector with n design variables, chosen randomly values within their domain, each individual is evaluated with the objective function. Equation (1) shows the gene of the mth individual. In all generations there are N individuals.

$$y_m = (x_1, x_2, x_3, ..., x_n). \tag{1}$$

2. Selection of parents and crossover. In this step, the individuals of the t_i generation, with the best solution that minimizes the objective function are selected to perform crossover. The type of selection used corresponds to roulette selection, where the most outstanding individuals have a higher probability of being selected than the less outstanding individuals. Each individual evaluation by the objective function has a result, namely cost (c), a probability p_m is assigned to each individual y_m according to its c_m, using Eq. (2).

$$p_m = e^{-\beta(c_m/[1/N]\sum_m c_m)}, \tag{2}$$

where β is the selection pressure and

$$\sum_m p_m = 1, \tag{3}$$

$$c_m \leq c_k \Longleftrightarrow p_m \geq p_k, \tag{4}$$

must be satisfied. Two individuals, namely parents v_1 and v_2, are chosen randomly accordingly to its probability p_m, to perform crossover,

$$v_1 = (v_{11}, v_{12}, v_{13}, ..., v_{1n}), \tag{5}$$

$$v_2 = (v_{21}, v_{22}, v_{23}, ..., v_{2n}). \tag{6}$$

Each crossover creates two offspring, u_1 and u_2,

$$u_1 = (u_{11}, u_{12}, u_{13}, ..., u_{1n}), \tag{7}$$

$$u_2 = (u_{21}, u_{22}, u_{23}, ..., u_{2n}), \tag{8}$$

accordingly, to Eqs. (9) and (10).

$$u_{1j} = \alpha_j v_{1j} + (1 - \alpha_j) v_{2j}, \tag{9}$$

$$u_{2j} = \alpha_j v_{2j} + (1 - \alpha_j) v_{1j}, \tag{10}$$

in which

$$\alpha = (\alpha_1, \alpha_2, \alpha_3, ..., \alpha_n), \tag{11}$$

with

$$\alpha_j \in [-\gamma, 1 + \gamma], \gamma \in \mathbb{R}. \tag{12}$$

The selection of parents and the creation of offspring are executed until the number of offspring required N_{of} is achieved.

3. Mutation. In this step, each offspring has a probability of changing some of the values of their gene, within a certain allowed range for each design variable, this process creates a changed version of the offspring, Eq. (13). Some design variables of the gene of the offspring are chosen randomly to change its value accordingly to Eq. (14).

$$u_m \rightarrow u'_m, \tag{13}$$

$$u'_{mj} = u_{mj} + \delta, \tag{14}$$

where δ it is a number selected by a normal probability distribution with mean $\mu = 0$ and selectable variance σ^2.

4. Union of population and offspring. In this step, the current population (t_i) is joined with the offspring generated in the selection of parents and crossover step, giving a population size of $N + N_{of}$.

5. Evaluation and selection. In this step, the N_{of} offspring population is evaluated with the objective function, and the population $N + N_{of}$ is ordered accordingly to the individuals c_m to select the best N individuals, these individuals generate the population of the generation t_{i+1}.

6. Termination. In this step, it is determined whether it is necessary to end the evolutionary loop or to return to the Selection of parents and crossover step. The termination is done when the evolutionary loop reaches a maximum number of iteration (MaxIt), this is t_{MaxIt}.

The GA parameters used in this work correspond to, MaxIt= 50; $N = 10$; $N_{of} = N$; $\beta = 1$; $\gamma = 0.25$ and $\sigma = 0.4$. An in-house software based on Phyton, from the Python Software Foundation [45] (with headquarters in Delaware, USA), was developed to execute the GA.

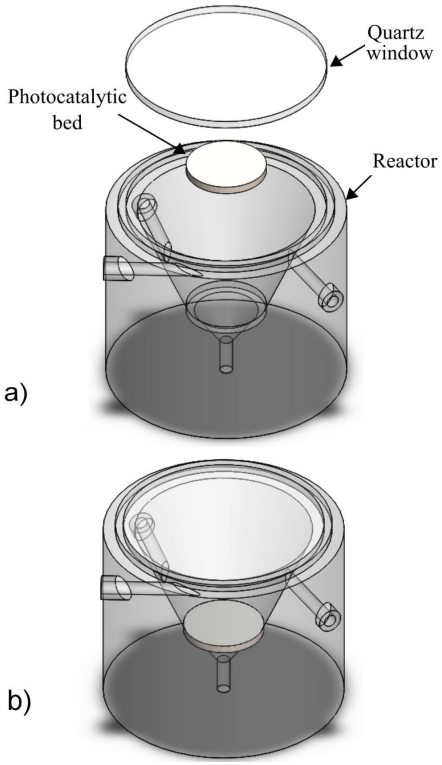

FIGURE 1. Multi-inlet vortex photoreactor components for Genetic Algorithm optimization: a) Exploded view of the multi-inlet vortex photoreactor components; b) Assembly of the multi-inlet vortex photoreactor components.

2.1.2. *Design Variables and Boundary Conditions*

The proposed multi-inlet photoreactor, namely GA photoreactor, consists of three main components. First, a quartz window is located in the upper part that allows the passage of light. Second, a photocatalytic bed is placed in the lower part of the main chamber before the reactor outlet (the photocat-

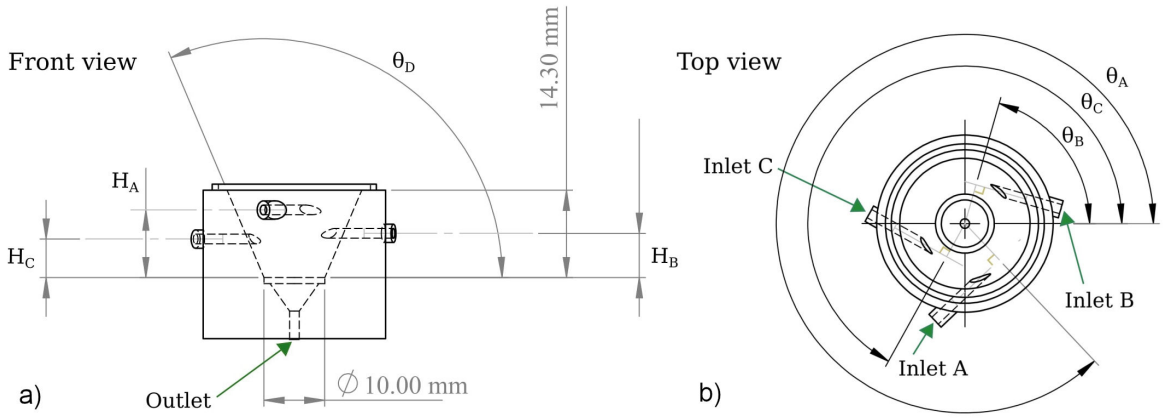

FIGURE 2. Design variables for the Genetic Algorithm: a) Shows the three design variables related to the height H of the reactant inlets as well as the design variable that controls the angled wall of the main chamber θ_D; b) Shows those design variables related to reactants inlets angle (θ_A, θ_B, and θ_C) around the main chamber.

TABLE I. Limit values for the reactor design variables.

Name	Maximum Value	Minimum Value
θ_A	360.0°	310.0°
θ_B	168.0°	70.0°
θ_C	288.0°	190.0°
θ_D	150.0°	90.0°
H_A	13.5 mm	2.0 mm
H_B	13.5 mm	2.0 mm
H_C	13.5 mm	2.0 mm

alytic bed, for the CFD is isotropic with a porosity of 50% and a width of 1 mm). And, third, the reactor body where the main chamber is surrounded by the reactant gas inlets. Figure 1 shows the detail of the different parts of the photoreactor.

The geometric design variables, that modify the current GA photoreactor, add up to seven, refer to Fig. 2. Three design variables correspond to the angle around the main chamber of the three inlets, namely θ_A, θ_B, and θ_C. These inlets are always tangent to the circle formed by the cut of the cone at their specific height, and have a diameter of 1.59 mm. Another three design variables are the height of the inlets, namely H_A, H_B and H_C, all the heights are measured from the surface of the photocatalytic bed. Finally, the angle of the wall in the main chamber, which is labeled as θ_D.

Only two dimensions are kept constant, the height of the main chamber, with a value of 14.30 mm, and the diameter of the photocatalytic bed, with a value of 10 mm. The gene of the *mth* individual in the GA will be,

$$y_m = (\theta_A, \theta_B, \theta_C, \theta_D, H_A, H_B, H_C). \tag{15}$$

The maximum and minimum values for the design variables are shown in Table I. The limit values for θ_A, θ_B, and θ_C were selected to ensure no superposition of the inlets.

The objective function corresponds to the volume rate (Φ_{Vf} ml/min) that passes through the photocatalytic bed. In all the runs for the GA the three inlets have a volume flow rate of 83.3 ml/min with CO_2 at 298 K, and the outlet has a pressure opening at 100 kPa, as boundary conditions for the CFD. A Flow chart for the implemented GA is shown in Fig. 3.

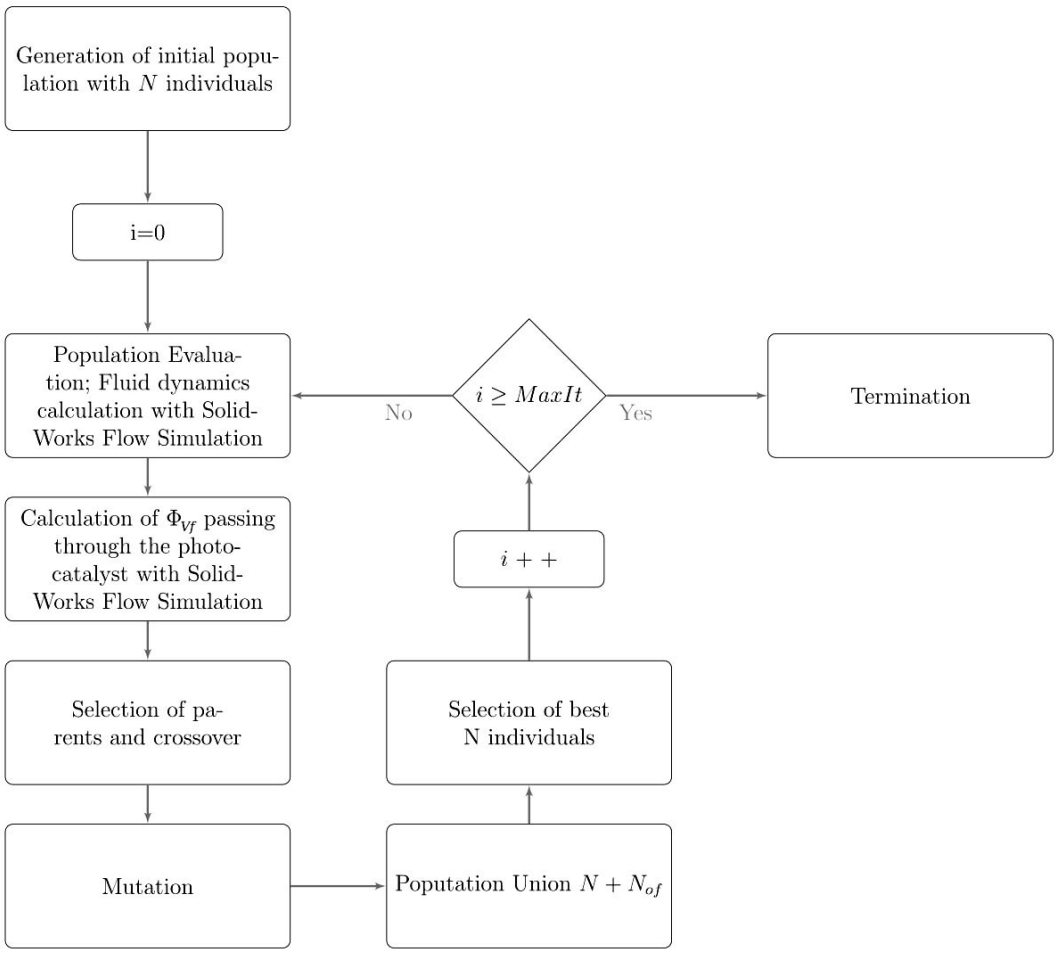

FIGURE 3. Genetic algorithm flow chart.

2.1.3. *Computational Fluid Dynamics*

All CFD software includes a representation of the Navier-Stokes equations, turbulence models and models that represent physical phenomena. In this work, the CFD software that was selected corresponds to SolidWorks Flow Simulation from $Dassault\ \ Systèmes$, with headquarters in Vélizy-Villacoublay, France. This tool uses a modified $k-\varepsilon$ two-equation turbulence model designed to simulate accurately a wide range of turbulence scenarios, and a boundary Cartesian meshing technique that allows accurate flow field resolution with low cell mesh densities.

Depending on the tested fluid and its conditions, any fluid flow can be classified as one of the following [46]:

- Laminar. That is, a smooth flow without any disturbances.
- Turbulent. This is a flow regime characterized by random vorticity and Eddie currents.
- Transitional. An alternation between laminar and turbulent regions.

The modified $k-\varepsilon$ turbulence model with damping functions proposed by Lam and Bremhorts, and used in SolidWorks Flow Simulation, describes laminar, turbulent and transitional flows of homogeneous fluids. This model employs two transport equations, one for the turbulent kinetic energy (k), Eq. (16), and the second for the turbulent dissipation (ε), Eq. (17) [47].

$$\frac{\partial \rho k}{\partial t}+\frac{\partial \rho k u_i}{\partial t}=\frac{\partial}{\partial x_i}\left(\left[\mu+\frac{\mu_t}{\sigma_k}\right]\frac{\partial k}{\partial x_i}\right) + \tau_{ij}^R\frac{\partial u_i}{\partial x_i}-\rho\varepsilon+\mu_t P_B, \tag{16}$$

$$\frac{\partial \rho \varepsilon}{\partial t}+\frac{\partial \rho \varepsilon u_i}{\partial t}=\frac{\partial}{\partial x_i}\left(\left[\mu+\frac{\mu_t}{\sigma_\varepsilon}\right]\frac{\partial \varepsilon}{\partial x_i}\right) +C_{\varepsilon 1}\frac{\varepsilon}{k}\left(f_1\tau_{ij}^R\frac{\partial u_i}{\partial x_j}+C_B\mu_t P_B\right)-f_2 C_{\varepsilon 2}\frac{\rho\varepsilon^2}{k}, \tag{17}$$

with

$$\tau_{ij}=\mu s_{ij}, \tag{18}$$

$$\tau_{ij}^R=\mu_t s_{ij}-\frac{2}{3}\rho k\delta_{ij}, \tag{19}$$

$$s_{ij}=\frac{\partial u_i}{\partial x_j}+\frac{\partial u_j}{\partial x_i}-\frac{2}{3}\delta_{ij}\frac{\partial u_k}{\partial x_k}, \tag{20}$$

$$P_B=-\frac{g_i}{\sigma_B}\frac{1}{\rho}\frac{\partial \rho}{\partial x_i}, \tag{21}$$

in which, $C_\mu=0.09$, $C_{\varepsilon 1}=1.44$, $C_{\varepsilon 2}=1.92$, $\sigma_\varepsilon=1.30$, $\sigma_B=0.90$, $C_B=1.00$ if $P_B>0$ and $C_B=0.00$ if $P_B<0$.

The turbulent viscosity is determined by:

$$\mu_t=f_\mu\frac{C_\mu\rho k^2}{\varepsilon}. \tag{22}$$

The Lam and Bremhorst's damping function f_μ is determined by:

$$f_\mu=\left(1-e^{-0.025R_y}\right)^2\left(1+\frac{20.5}{R_t}\right), \tag{23}$$

where,

$$R_y=\frac{\rho\sqrt{ky}}{\mu}, \tag{24}$$

$$R_t=\frac{\rho k^2}{\mu\varepsilon}. \tag{25}$$

In this case, y is the distance from a point to the wall and Lam and Bremhorst's damping functions f_1 and f_2 are determined by:

$$f_1=1+\left(\frac{0.05}{f_\mu}\right)^3, \tag{26}$$

$$f_2=1-e^{R_i^2}. \tag{27}$$

The heat flux is defined by:

$$q_i=\left(\frac{\mu}{Pr}+\frac{\mu_t}{\sigma_c}\right)\frac{\partial h}{\partial x_i}, \qquad i=\{1,2,3\}, \tag{28}$$

where, $\sigma_c=0.9$, Pr is the Prandtl Number, and h is the thermal enthalpy.

Another important quantity for analysis is the turbulence intensity, which is defined as,

$$I\equiv\frac{u'}{U}, \tag{29}$$

where u' is the root-mean-square of the turbulent velocity fluctuations and U is the mean velocity (Reynolds averaged), and can be computed as

$$I\equiv\sqrt{\frac{1}{3}\left({u'_x}^2+{u'_y}^2+{u'_z}^2\right)}=\sqrt{\frac{1}{3}k}, \tag{30}$$

the mean velocity can be obtained from the three mean velocity components as

$$U\equiv\sqrt{\frac{1}{3}\left({u_x}^2+{u_y}^2+{u_z}^2\right)}. \tag{31}$$

For each reactor design a global mesh of level 4, with an advanced channel refinement provided by SolidWorks Flow Simulation, was used for the determination of the fluid dynamics. The solver was configured to reach a steady-state.

For comparative purposes, a reference photoreactor was studied. The geometrical consideration for this reference photoreactor was of those from the classical configuration for multi-inlet vortex reactors [48, 49]. In this reference reactor, gas feed inlets are at equidistant position each other and their heights are at the middle of the main cylinder, see Fig. 4. The

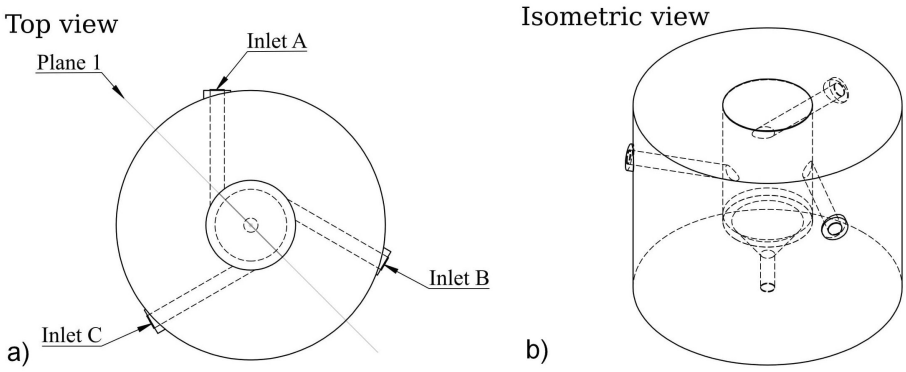

FIGURE 4. Reference reactor inlets configuration: a) Inlets and plane 1 for the cut plot. b) Isometric view of the reference photoreactor.

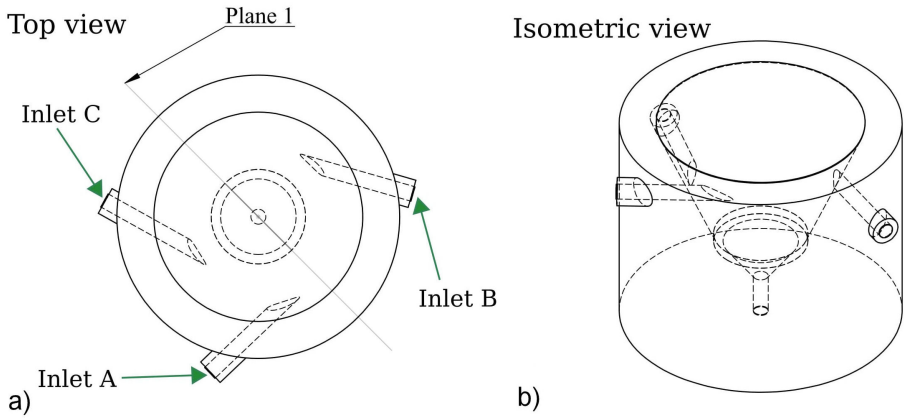

FIGURE 5. Optimized photoreactor inlets configuration: a) Inlets and plane 1 for the cut plot. b) Isometric view of the optimized photoreactor.

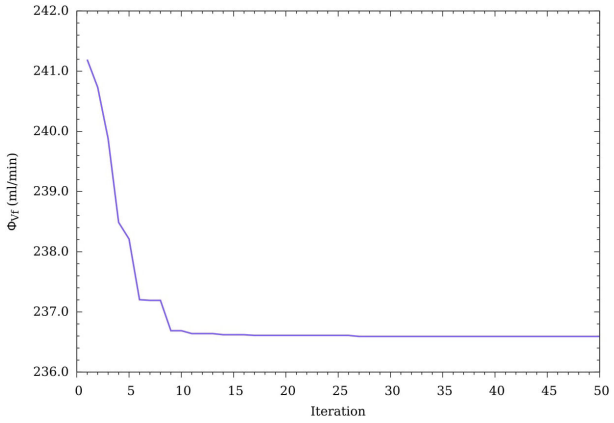

FIGURE 6. Calculated volumetric flow rate passing through photocatalytic bed after several iterations for the optimization process using GA.

criteria to evaluate the performance of both the optimized configuration of the prototype photoreactor and the reference, are the value of the turbulence and the residence time average. Because of this, a plane that cuts transversally both reactors is used, namely plane 1, this plane is depicted in Figs. 4 and 5 for optimized and reference photoreactor respectively.

3. Results and discussion

3.1. Genetic algorithm

Throughout the optimization process, 500 reactor designs were simulated, and for each iteration of the evolutionary loop, the value of the best reactor desing Φ_{Vf} was obtained and plotted (Fig. 6). For the first five iterations there is a sharp decrease of Φ_{Vf}, suggesting a good performance of the GA. After iteration number ten, it can be seen that there is a

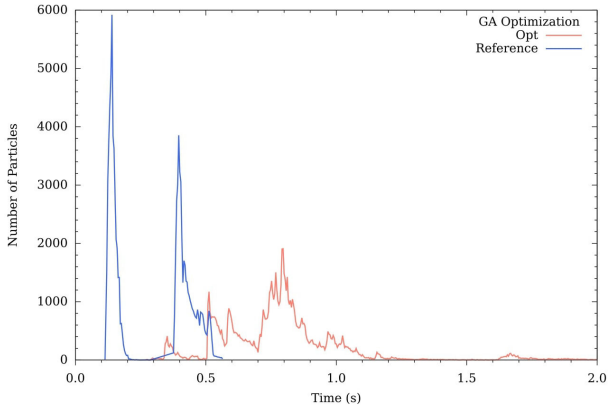

FIGURE 7. Residence time distribution for the Opt photoreactor and the reference photoreactor.

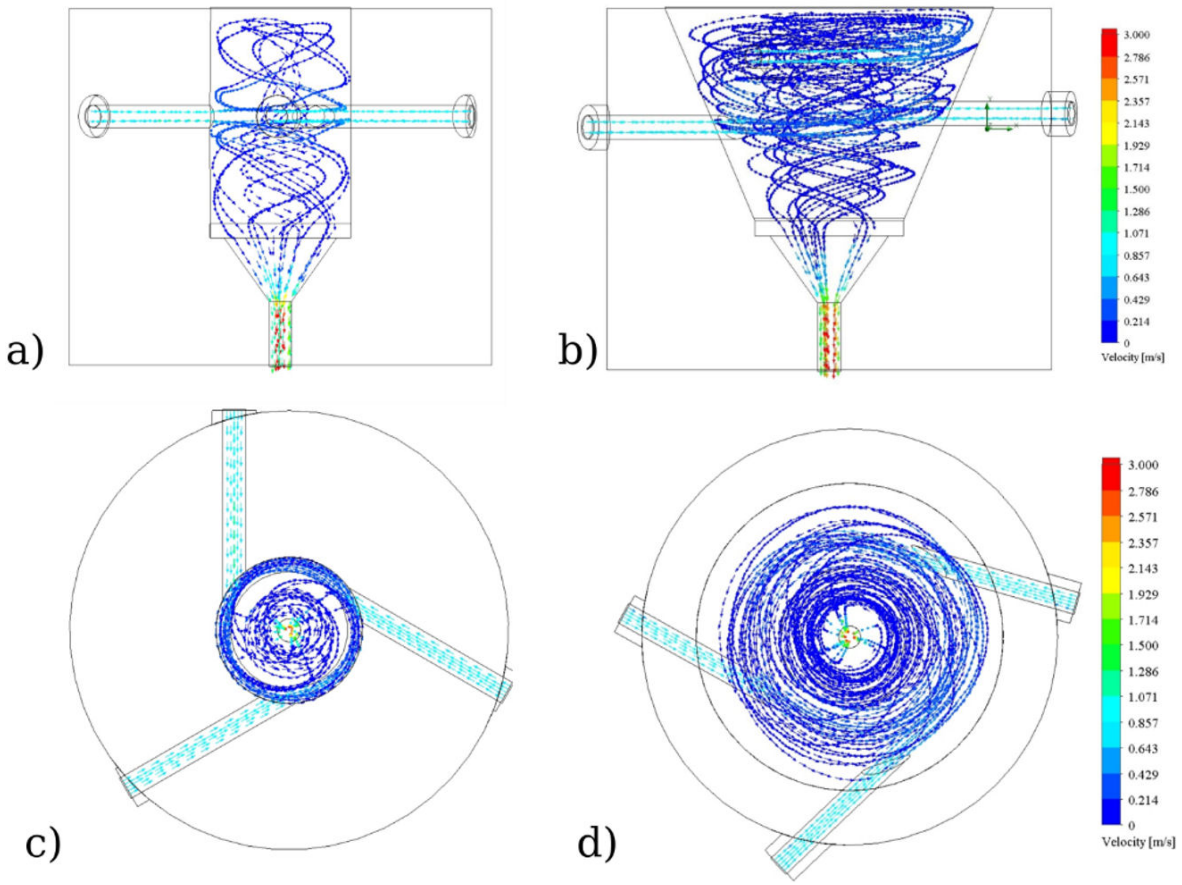

FIGURE 8. Flow trajectories: a) Reference photoreactor front view; b) Opt-3-Tuned photoreactor front view; c) Reference photoreactor top view; d) Opt-3-Tuned photoreactor top view.

TABLE II. The optimized set of parameters for the reactor configuration, taken as indicated in Fig. 2.

Name	Value
θ_A	313.4°
θ_B	74.0°
θ_C	240.9°
θ_D	113.0°
H_A	11.0 mm
H_B	7.20 mm
H_C	6.30 mm

slight change of Φ_{Vf}, indicating a local minimum approximation in the design space. After iteration number thirty there is no change in the Φ_{Vf} value, and the algorithm reaches a local minimum. The final values of the design variables are shown in Table II.

3.2. Residence time distribution and turbulence intensity

In order to find the residence time distribution for the optimized photoreactor (Opt) and the reference photoreactor a particle study was performed, where 30,000 representative particles of CO_2 fluid were injected at each inlet, with a volume flow rate of 83.3 ml/min for all the three inlets. Figure 7 shows the residence time distribution for both photoreactors, it can be noted that the Opt photoreactor has a more uniform distribution with particles that stays longer in the reactor than the reference photoreactor. Also, the reference photoreactor has two main regions of time, the first between 0.1 s and 0.2 s, and the second, between 0.3 s and 0.6 s, whereas for the Opt photoreactor the main time region is between 0.5 s and 1.1 s. The mean residence time for the Opt photoreactor corresponds to 0.79 s, and for the reference photoreactor 0.29 s, this is an improvement of 2.7 times with respect of the reference photoreactor. This proves that with Φ_{Vf} as the objective function for the GA implementation, it is possible to adjust indirectly the residence time for this type of photoreactors.

Figure 8 shows the flow trajectories for the reference photoreactor and the Opt photoreactor. It can be seen from Figs. 8a) and 8b) that the higher part of the Opt photoreactor has more fluid lines than the reference photoreactor, this is an indication of better reactants distributions inside the Opt photoreactor. Figures 8c) and 8d) show the vortex formed in both photoreactors. It can be noted that the fluid trajectories for the reference reactor are concentrated near the cylinder wall, whereas for the Opt photoreactor its fluid trajectories are more concentrated at the middle of the cone wall. More-

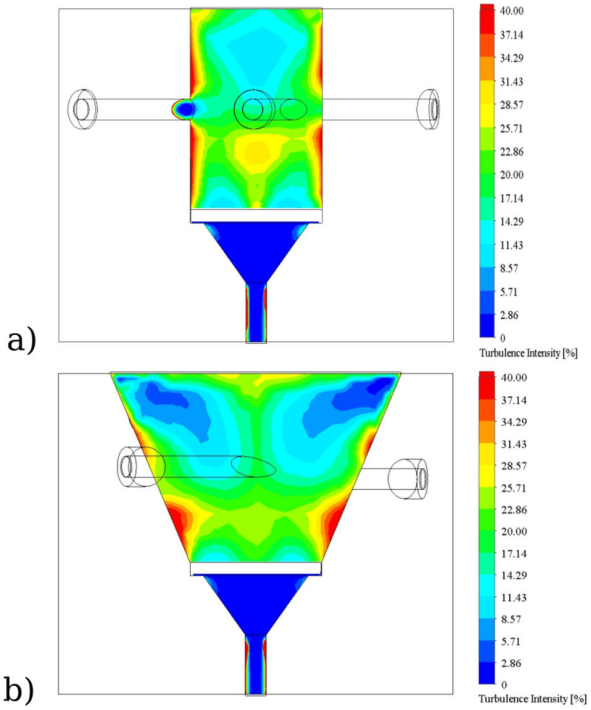

FIGURE 9. Flow trajectories: a) Reference photoreactor front view; b) Opt-3-Tuned photoreactor front view.

over, it can be seen from this figure that molecules have to travel longer path in the Opt photoreactor, this has consequently that residence time becomes longer because of these larger trajectories within this optimized photoreactor.

A cut plot on plane 1, showed in Figs. 9a) and b), was performed to find the turbulence intensities behavior inside both photoreactors. It can be observed that there are marked turbulent zones (more than 10%) near the photocatalytic bed in both cases. The case of the reference photoreactor reaches 14.5% turbulence intensity on the photocatalytic bed surface, whereas for the Opt photoreactor the average turbulence intensity onto the photocatalytic bed yields 15.5%. This turbulence intensity of the Opt photoreactor together with the high turbulence intensity near the photocatalytic bed ensures the mixing and contact of the reactant phases.

4. Conclusions

Computational Fluid Dynamics showed goodness in process operation and optimization in order to gain insight into the performance of a current designed and tailored photoreactor configuration. According to the simulation results, by changing the inlet angles and height, as well as the wall angle of the main chamber in the photoreactor, a higher residence time and turbulence are enhanced that, logically, in a multiphase system such as our planned reaction system, is essential for the reaction to occur. With the current study, reactor design and optimization lead to construct the physical device to perform the experimental study with the conviction that its performance will be optimal and the kinetic measurements will be intrinsic. The latter is the target of our further work and research.

Funding

This work was partially funded by Universidad Autónoma de Querétaro grants number UAQ-PTC-390 PRODEP, FCQ202002 and FONDEC-UAQ-FCQ-202004. J.V. thanks to CONACYT scholarship number 705989. J.L.D.J. wish to thank the financial support from CATEDRAS-CONACYT, grant number 1039 and CONACYT-A1-S-8317.

1. R. A. Betts, C. D. Jones, J. R. Knight, R. F. Keeling, and J. J. Kennedy, El Nino and a record CO_2 rise. *Nature Climate Change* **6** (2016) 806, https://doi.org/10.1038/nclimate3063.

2. R. K. Pachauri *et al.*, Climate Change 2014: Synthesis Report. Contribution of Working Groups I, II and III to the Fifth Assessment Report of the Intergovernmental Panel on Climate Change. IPCC, 2014.

3. B. Looney, *Statistical Review of World Energy*, *British Petroleum* **69** (2020) 66.

4. A. Mustafa, B. G. Lougou, Y. Shuai, Z. Wang, and H. Tan, Current technology development for CO_2 utilization into solar fuels and chemicals: A review. *Journal of Energy Chemistry* **49** (2020) 96, https://doi.org/10.1016/j.jechem.2020.01.023.

5. S. Zhang, Q. Fan, R. Xia, and T. Meyer, CO_2 reduction: from homogeneous to heterogeneous electrocatalysis. *Accounts Of Chemical Research*, **53** (2020) 255, https://doi.org/10.1021/acs.accounts.9b00496.

6. G. Zhao, X. Huang, X. Wang, and X. Wang, Progress in catalyst exploration for heterogeneous CO_2 reduction and utilization: a critical review. *Journal Of Materials Chemistry A* **5** (2017) 21625 https://doi.org/10.1039/c7ta07290b.

7. J. Schneider, H. Jia, J. Muckerman, and E. Fujita, Thermodynamics and kinetics of CO_2, CO, and H+ binding to the metal centre of CO_2 reduction catalysts. *Chemical Society Reviews*, **41** (2012) 2036, https://doi.org/10.1039/c1cs15278e.

8. Y. J. Zhou, E. J. Kerkhoven, and J. Nielsen, Barriers and opportunities in bio-based production of hydrocarbons. *Nature Energy*. **3** (2018) 925, https://doi.org/10.1038/s41560-018-0197-x.

9. K. S. Adarsh, N. Chandrasekaran, and V. Chakrapani, In-situ spectroscopic techniques as critical evaluation tools for electrochemical carbon dioxide reduction: a mini review. *Frontiers In Chemistry*. **8** (2020) 137, https://doi.org/10.3389/fchem.2020.00137.

10. M.-Y. Lee *et al.*, Current achievements and the future direction of electrochemical CO_2 reduction: A short review. *Crit-*

ical Reviews In Environmental Science And Technology. **50** (2020) 769, https://doi.org/10.1080/10643389.2019.1631991.

11. J. Gong, C. Li, and M. R. Wasielewski, Advances in solar energy conversion. *Chemical Society Reviews*. **48** (2019) 1862 https://doi.org/10.1039/c9cs90020a.

12. N. Lewis, Toward cost-effective solar energy use. *Science*. **315** (2007) 798, https://doi.org/10.1126/science.1137014.

13. N.-N. Vu, S. Kaliaguine, and T.-O. Do, Plasmonic Photocatalysts for Sunlight-Driven Reduction of CO_2: Details, Developments, and Perspectives. *Chem. Sus. Chem*. **13** (2020) 3967, https://doi.org/10.1002/cssc.202000905.

14. K. Li, B. Peng, and T. Peng, Recent advances in heterogeneous photocatalytic CO_2 conversion to solar fuels, *ACS Catalysis*. **6** (2016) 7485, https://doi.org/10.1021/acscatal.6b02089.

15. M.A. Green and S.P. Bremner, Energy conversion approaches and materials for high-efficiency photovoltaics. *Nature Materials* **16** (2017) 23 , https://doi.org/10.1038/nmat4676.

16. S. Zhu, and D. Wang, Photocatalysis: basic principles, diverse forms of implementations and emerging scientific opportunities, *Adv. Ener. Mater.*. **7** (2017) 1700841 https://doi.org/10.1002/aenm.201700841.

17. R. Shi, and Y. Chen, Controlled formation of defective shell on TiO_2 (001) facets for enhanced photocatalytic CO_2 reduction. *Chem. Cat. Chem*. **11** (2019) 2270 https://doi.org/10.1002/cctc.201900061.

18. K. Li, C. Teng, S. Wang, and Q. Min, Recent advances in TiO_2-based heterojunctions for photocatalytic CO_2 reduction with water oxidation: A review. *Frontiers In Chemistry* **9** (2021) 637501, https://doi.org/10.3389/fchem.2021.637501.

19. F. O. Ochedi, D. Liu, J. Yu, A. Hussain, and Y. Liu, Photocatalytic, electrocatalytic and photoelectrocatalytic conversion of carbon dioxide: a review. *Environmental Chemistry Letters* **19** (2020) 941, https://doi.org/10.1007/s10311-020-01131-5.

20. S. Zeng, P. Kar, U. Thakur, and K. Shankar, A review on photocatalytic CO_2 reduction using perovskite oxide nanomaterials. *Nanotechnology* **29** (2018) 052001 https://doi.org/10.1088/1361-6528/aa9fb1.

21. T. Kistler, *et al.*, Integrated Membrane-Electrode-Assembly Photoelectrochemical Cell under Various Feed Conditions for Solar Water Splitting. *Journal Of The Electrochemical Society*. **166** (2018) H3020, https://doi.org/10.1149/2.0041905jes.

22. H. Kim, A. Razzaq, H. Heo, and S. In, Photocatalytic conversion of CO_2 into hydrocarbon fuels with standard titania (Degussa P25) using newly installed experimental setup. *Rapid Communication In Photoscience*. **2** (2013) 64, https://doi.org/10.5857/rcp.2013.2.2.64.

23. C. Passalía, O. M. Alfano, and R. J. Brandi, Integral design methodology of photocatalytic reactors for air pollution remediation. *Molecules*. **22** (2017) 945, https://doi.org/10.3390/molecules22060945.

24. P. J. Valadés-Pelayo, *et al.*, A. Effect of photocatalyst film geometry on radiation absorption in a solar reactor, a multiscale approach. *Chemical Engineering Science*. **161** (2017) 24 https://doi.org/10.1016/j.ces.2016.11.046.

25. M. Mueses, J. Colina-Márquez, F. Machuca-Martínez, and G. Puma, Recent advances on modeling of solar heterogeneous photocatalytic reactors applied for degradation of pharmaceuticals and emerging organic contaminants in water. *Current Opinion In Green And Sustainable Chemistry* **30** (2021) 100486 https://doi.org/10.1016/j.cogsc.2021.100486.

26. P. J. Valadés-Pelayo, F. G. Sosa, B. Serrano, and H. De Lasa, Eight-lamp externally irradiated bench-scale photocatalytic reactor: Scale-up and performance prediction. *Chem. Eng. J.* **282** (2015) 142, https://doi.org/10.1016/j.cej.2015.03.039.

27. S. Ali *et al*., Gas phase photocatalytic CO_2 reduction,"A brief overview for benchmarking". *Catalysts*. **9** (2019) 727, https://doi.org/10.3390/catal9090727.

28. P. Mazierski, B. Bajorowicz, E. Grabowska, and A. Zaleska-Medynska, Photoreactor design aspects and modeling of light. *Heterogeneous Photocatalysis* (Springer, Berlín, 2016) 211, https:/doi.org/10.1007/978-3-662-48719-8_7.

29. M. Dilla, R. Schlögl, and J. Strunk, Photocatalytic CO_2 Reduction Under Continuous Flow High-Purity Conditions: Quantitative Evaluation of CH_4 Formation in the Steady-State. *Chem. Cat. Chem*. **9** (2017) 696, https://doi.org/10.1002/cctc.201601218.

30. D. Simon, Evolutionary optimization algorithms. (John Wiley and Sons, 2013).

31. D. Goldberg, and J. Holland, Genetic algorithms and machine learning, *Machine Learning 3* (1988) 95.

32. K. De Jong, Analysis of the behavior of a class of genetic adaptive systems *Technical Report* No. 185, Department of Computer and Communication Sciences, University of Michigan (1975).

33. J. M. Johnson, and Y. Rahmat-Samii, Genetic algorithm optimization and its application to antenna design. *Proceedings Of IEEE Antennas And Propagation Society International Symposium And URSI National Radio Science Meeting*. **1** (1994) 326, https://doi.org/10.1109/APS.1994.407746.

34. C. Casado, J. Marugán, R. Timmers, M. Muñoz, and R. Grieken, Comprehensive multiphysics modeling of photocatalytic processes by computational fluid dynamics based on intrinsic kinetic parameters determined in a differential photoreactor. *Chemical Engineering Journal*. **310** (2017) 368, https://doi.org/10.1016/j.cej.2016.07.081.

35. J. Dedeyne, *et al*., Computational fluid dynamics-based optimization of dimpled steam cracking reactors for reduced CO_2 emissions. *AIChE Journal*. **66** (2020) e16255, https://doi.org/10.1002/aic.16255.

36. M. T. Akram, and M.-H. Kim, CFD Analysis and Shape Optimization of Airfoils Using Class Shape Transformation and Genetic Algorithm Part I. *Applied Sciences*. **11** (2021) 3791, https://doi.org/10.3390/app11093791.

37. T. Norton and D.-W. Sun, Computational fluid dynamics (CFD)-an effective and efficient design and analysis tool for the food industry: a review. *Trends In Food Science & Technology*. **17** (2006) 600, https://doi.org/10.1016/j.tifs.2006.05.004.

38. A. G. Dixon, and M. Nijemeisland, CFD as a design tool for fixed-bed reactors. *Industrial & Engineering Chemistry Research*. **40** (2001) 5246, https://doi.org/10.1021/ie001035a.

39. S. Kulkarni, *et al.*, Computational fluid dynamics-assisted process intensification study for biomass fast pyrolysis in a gas-solid vortex reactor. *Energy & Fuels*. **32** (2018) 10169, https://doi.org/10.1021/acs.energyfuels.8b01008.

40. D. Lee, *et al.*, Continuous photo-oxidation in a vortex reactor: efficient operations using air drawn from the laboratory. *Organic Process Research & Development*. **21** (2017) 1042, https://doi.org/10.1021/acs.oprd.7b00153.

41. K. Tong, L. Yang, X. Du, and Y. Yang, Review of modeling and simulation strategies for unstructured packing bed photoreactors with CFD method. *Renewable And Sustainable Energy Reviews*. **131** (2020) 109986, https://doi.org/10.1016/j.rser.2020.109986.

42. D. J. Rader, Deterministic operations research: models and methods in linear optimization. (John Wiley and Sons, 2010).

43. S. Norving, and P. Russel, *Artificial Intelligence A Modern Approach.* (Prentice Hall Upper Saddle River, NJ, USA, 2002).

44. L. M. Schmitt, Theory of genetic algorithms. *Theoretical Computer Science*. **259** (2001) 1, https://doi.org/10.1016/s0304-3975(00)00406-0.

45. G. Van Rossum, and F. Drake Jr, *Python tutorial.* (Centrum voor Wiskunde en Informatica Amsterdam, 1995).

46. H. Schlichting and E. Truckenbrodt, Aerodynamik des Flugzeuges Grundlagen aus der Strömungsmechanik Aerodynamik des Tragflügels (Teil I). (Springer, 1959).

47. C. K. G. Lam, and K. Bremhorst, A modified form of the $k-\varepsilon$ model for predicting wall turbulence, *J. Fluids Eng.* 103 (1981) 456, https://doi.org/10.1115/1.3240815.

48. Z. Liu, A. Passalacqua, M. Olsen, R. Fox, and J. Hill, Dynamic delayed detached eddy simulation of a multi-inlet vortex reactor. *AIChE Journal* **62** (2016) 2570. https://doi.org/10.1002/aic.15230.

49. R. Fang, *et al.*, Large-scale synthesis of lipid-polymer hybrid nanoparticles using a multi-inlet vortex reactor. *Langmuir*. **28** (2012) 13824. https://doi.org/10.1021/la303012x.